Dual-mode behavior of the complementary electric-LC resonators loaded on transmission line: Analysis and applications

Amir Ebrahimi,[a] Withawat Withayachumnankul,[b] Said F. Al-Sarawi,[c] and Derek Abbott[d]
School of Electrical and Electronic Engineering, The University of Adelaide, SA 5005, Australia

(Received 9 July 2014; accepted 11 August 2014; published online 26 August 2014)

This article presents an analysis of metamaterial resonators coupled with microstrip transmission line. The behavior of complementary electric-LC resonators loaded on a microstrip line is analyzed using the equivalent circuit model. In this paper, it is shown that a special type of these resonators show a dual-mode behavior when excited through the electromagnetic field around the microstrip transmission lines. The bandstop and bandpass configurations of these dual mode resonators loaded with microstrip lines are introduced and analyzed. Their potential applications are highlighted through designing a displacement sensor and a dual-mode bandpass filter prototypes. © *2014 AIP Publishing LLC*. [http://dx.doi.org/10.1063/1.4893751]

I. INTRODUCTION

Transmission lines loaded with split-ring resonators (SRRs) and complementary split-ring resonators (CSRRs) have been widely used in designing new metamaterial-based devices.[1] In these structures, the resonators are excited through nonuniform electric/magnetic fields of the transmission lines. Depending on their topology, the resonator-loaded transmission lines can exhibit different properties such as bandstop, bandpass, left/right handed wave propagation suitable for different applications. Metamaterial transmission lines made of SRR loaded coplanar waveguide (CPW) and CSRR-loaded microstrip lines have been introduced.[2,3] Later on, many improved bandpass and bandstop planar filters based on SRR or CSRR-coupled transmission lines have been developed.[4–6] The high quality factor resonance and high sensitivity of the SRRs and CSRRs to the geometrical and environmental changes are used for designing microwave planar sensors.[7–9] Note that SRRs and CSRRs are also applied as loading elements in designing differential microstrip lines[10] and several improved antenna designs.[11,12]

Recently, electric-LC (ELC) resonators shown in Fig. 1 and their complementary counterparts (CELC) in Fig. 2 are utilized as loading elements for planar transmission lines.[13–15] The ELC resonators in Fig. 1 and their complementary structures in Fig. 2 are bisymmetric resonators since they show two symmetry planes, where one of them acts as an electric wall, while the other acts as a magnetic wall at the fundamental resonance frequency.[16–19] The resonators in Fig. 1 cannot be excited by the uniform out-of-plane (z oriented) magnetic field to access the fundamental resonance mode because the induced currents in the two loops of the resonator will cancel each other in the middle branch preventing the existence of a magnetic dipole moment in the z direction. However, they can be driven by an in-plane (y oriented) uniform electric field, which provides an electric dipole moment along the y axis. According to Babinet's principle, the complementary resonators in Fig. 2 can be driven by means of a uniform in-plane (y oriented) applied magnetic field but not through a uniform out-of-plane (z oriented) electric field at the fundamental resonance mode. These bisymmetric elements can also be excited by planar transmission lines where the fields are no longer uniform. They have been used by Naqui *et al.*[13] for suppression of the selective mode in microstrip differential lines, where different constructions with different orientations of the ELC or CELC have been studied and analyzed using lumped element circuit models. A CPW loaded with a single ELC resonator has been proposed by Naqui and Martín as an angular and velocity sensor.[15] In this sensor, rotation of the resonator with respect to the symmetry plane of the CPW leads to a change in coupling between the resonator and CPW. This in turn changes the notch depth in transmission response of the device. The rotation angle is then determined based on the notch depth of the transmission response. In Naqui *et al.*,[14] the loading of a single microstrip line with a CELC resonator has been considered and studied through an accurate circuit model. It has been shown that displacement of the CELC with respect to the microstrip causes a notch in the transmission response of the structure. Potential applications of this structure include generating RF barcodes, notch filters, and displacement sensors.

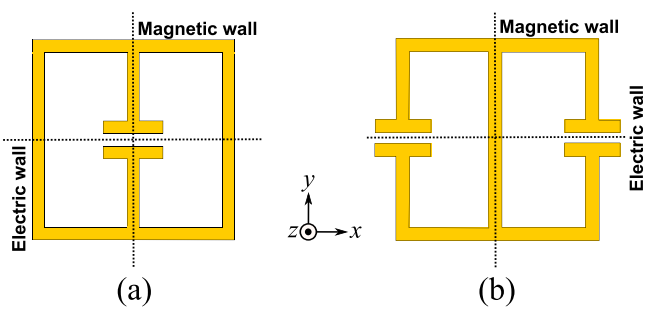

FIG. 1. Typical configurations of electric-LC (ELC) resonator. (a) ELC1 and (b) ELC2.

[a]Electronic mail: amir.ebrahimi@adelaide.edu.au
[b]Electronic mail: withawat.withayachumnankul@adelaide.edu.au
[c]Electronic mail: said.alsarawi@adelaide.edu.au
[d]Electronic mail: derek.abbott@adelaide.edu.au

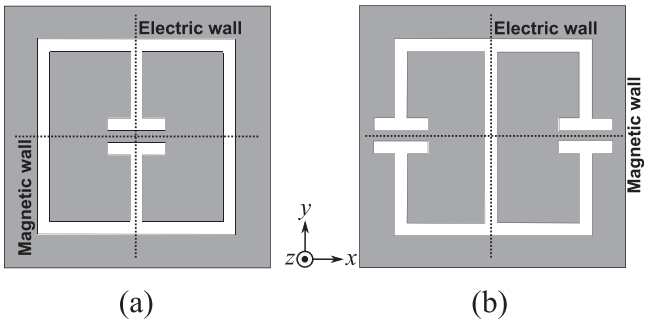

FIG. 2. Typical configurations of complementary electric-LC (CELC) resonator with the gray areas showing ground plane metalization. (a) CELC1 and (b) CELC2.

The resonators in Figs. 1 and 2(a) have been studied and reported in several previous articles.[13–15] On the other hand, an analysis of transmission lines loaded within Fig. 2(b) (called CELC2 here) is still lacking. A major difference between this resonator and the other ELC and CELC resonators lies in its subwavelength dual-mode behavior that makes it a very attractive choice for designing new compact microwave components. Here, we will provide an in-depth study of this dual-mode resonator through a lumped element circuit model. Additionally, different configurations of the microstrip-coupled resonator as well as their potential applications in planar microwave devices will be analyzed and explained.

Section II provides a brief introduction of the CELC2 resonator. The electromagnetic behavior of microstrip lines loaded with the CELC2 is studied through a circuit model in Sec. III. In Sec. IV, potential applications of the structures are demonstrated through designs of a displacement sensor and a dual-mode bandpass filter. Finally, Sec. V presents the work conclusions.

II. OPERATION PRINCIPLE OF CELC2 RESONATOR

Like the ELC1,2 and CELC1, the CELC2 resonator exhibits two symmetry planes, one of them acting as an electric wall, whereas the other one behaves as a magnetic wall. As discussed earlier, it can be excited by means of an in-plane (y oriented) applied magnetic field, but not through a uniform out-of-plane (z oriented) electric field. If the resonator dimensions are electrically small, it can be modelled by a lumped element equivalent circuit in Fig. 3(a). The parallel resonant branches of L_gC_g model the two halves of the resonator, where C_g presents the capacitive effect between the metallic halves and the surrounding ground plane and L_g models the inductive paths running from the two capacitive regions to the ground plane. Here, C_M stands for the mutual capacitive effect between the two metallic halves of the resonator. It can be inferred from this equivalent circuit that the particle can exhibit the even and odd-mode resonances with the equivalent circuits demonstrated in Figs. 3(b) and 3(c), respectively. In the even-mode, the two halves of the resonator have the same voltage distribution, and thus, no current will pass through C_M and it will be open-circuited. Conversely, in the odd-mode, there will be a virtual ground across the electric wall and C_M is broken into two equal parts of $2C_M$ as demonstrated in Fig. 3(c). Based on Fig. 3 and the above discussion, the even and odd-mode resonance frequencies of the resonator can be defined as

$$f_{\text{even}} = \frac{1}{2\pi\sqrt{L_gC_g}}, \tag{1}$$

$$f_{\text{odd}} = \frac{1}{2\pi\sqrt{L_g(C_g + 2C_M)}}. \tag{2}$$

As seen, in the odd-mode resonance, the C_M capacitor adds to the C_g causing a smaller resonance frequency with respect to the even-mode resonance.

III. MICROSTRIP LINE LOADED WITH CELC2 RESONATOR

As mentioned before, the CELC2 resonator can be excited through the fields generated by the planar transmission lines. This section is dedicated to the analysis of microstrip lines loaded with the CELC2 resonator. Both of the bandstop and bandpass configurations will be introduced and their electromagnetic behavior will be analyzed using equivalent circuit models.

A. Bandstop configuration

Here, the bandstop behavior of microstrip transmission line loaded with the CELC2 is explained using the circuit analysis. It should be emphasized that the equivalent circuit

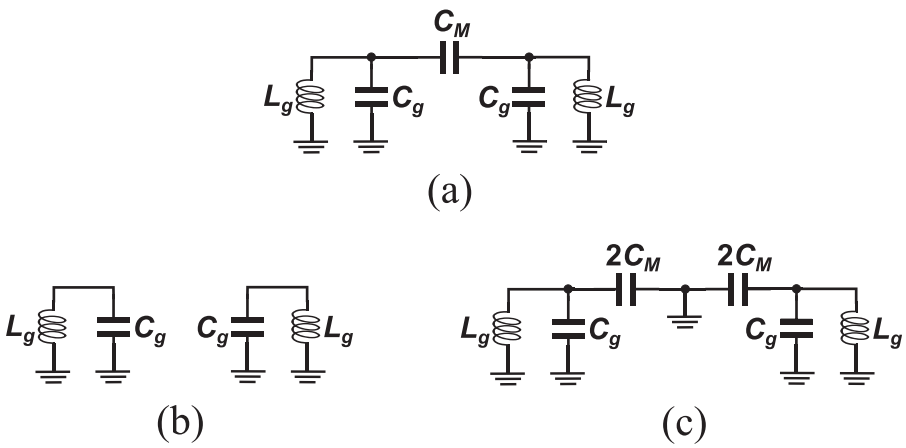

FIG. 3. Lumped element modeling of the CELC2. (a) Equivalent circuit model. (b) Even-mode circuit model. (c) Odd-mode circuit model.

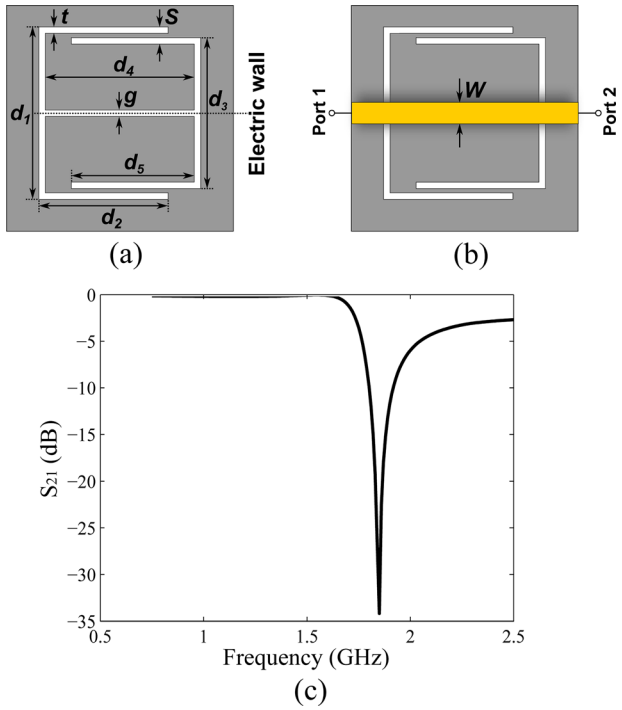

FIG. 4. Microstrip line loaded with CELC2 resonator. (a) Modified CELC2 resonator. (b) Modified CELC2 resonator coupled with the microstrip transmission line. (c) Transmission response when the resonator electric wall is aligned with the symmetry plane of the transmission line. The resonator and transmission line dimensions are: $d_1 = 10$ mm, $d_2 = 7.2$ mm, $d_3 = 9.4$ mm, $d_4 = 9.6$ mm, $d_5 = 7$ mm, $t = g = 0.2$ mm, and $S = 0.5$ mm. The considered substrate is Rogers RO6010 with $\epsilon_r = 10.2$ and $\tan\delta = 0.0023$ and a thickness of 1.27 mm.

analysis is valid as long as the unit cell dimension is electrically small.[20,21] In order to satisfy this condition, the resonator shown in Fig. 4(a) is considered instead of the one in Fig. 2(b). In Fig. 4(a), the magnetic wall no longer exists, but it still shows the behavior of the CELC2 resonator for the considered case. Fig. 4(b) shows a CELC2 resonator that is loaded onto a microstrip line with the electric wall of the resonator aligned with the symmetry plane of the transmission line. In this structure, since the two halves of the ELC2 are equally excited by the transmission line, they will share a same voltage distribution. Therefore, only the even-mode resonance will be excited and there will be just a single notch in the transmission response as shown in Fig. 4(c). This behavior can be also explained through the circuit model of the structure that is shown in Fig. 5(a). Here, the inductors L model the inductance associated with the microstrip, C_1 and C_2 present the coupling capacitances between the transmission line and the resonator, and R represents the losses. If the electric wall is aligned with the microstrip symmetry plane, the C_1 and C_2 coupling capacitors will be equal ($C_1 = C_2 = C$) and no current will pass through C_M. Hence, the equivalent circuit will be simplified to that shown in Fig. 5(b). Based on this model, the transmission notch occurs at a frequency that nulls the shunt impedance. Hence,

$$f_{\text{notch}} = \frac{1}{2\pi\sqrt{L_g(C_g + C)}}. \tag{3}$$

The values of circuit elements in Fig. 5(b) can be obtained using the procedure reported by Banache *et al.*[22] and Aznar *et al.*[23] that is based on characteristics of the transmission and reflection coefficients provided by electromagnetic simulations. There are four unknown parameters (L, C, L_g, and C_g) that can be calculated using the following four conditions: (i) The transmission notch frequency is the frequency in which the shunt impedance nulls as described by Eq. (3), (ii) the frequency for which the shunt impedance is open circuited corresponds to intersection between the reflection coefficient (S_{11}) and the normalized unit resistance circle in the Smith chart, (iii) the phase of transmission coefficient reaches (90°) when the series impedance is the complex conjugate of the shunt impedance, and (iv) the frequency at which the parallel admittance vanishes is the resonance frequency of the LC tank associated with the resonator. The resistance R can be determined by curve fitting of EM and circuit simulations. Fig. 6 shows a comparison between the electromagnetic and circuit-model simulations for a typical configuration in Fig. 4(b). The circuit parameters have been extracted through the procedure above. The plots demonstrate agreement between the EM and circuit simulations.

Now, if the symmetry planes of the transmission line and resonator are no longer aligned, C_1 and C_2 in Fig. 5(a) will take different values and this asymmetry allows current flowing through C_M. Hence, the odd-mode resonance will be excited causing another notch in the transmission response of the structure. The structure of Fig. 4(b) is simulated for three laterally displaced positions of the resonator with respect to the microstrip line (0.6 mm, 1 mm, and 2 mm). To extract the unknown elements of the equivalent circuit model of the displaced structure in Fig. 5(a), first, we consider the circuit elements for the aligned structure in Fig. 5(b) by using the four conditions described before. Then, the value

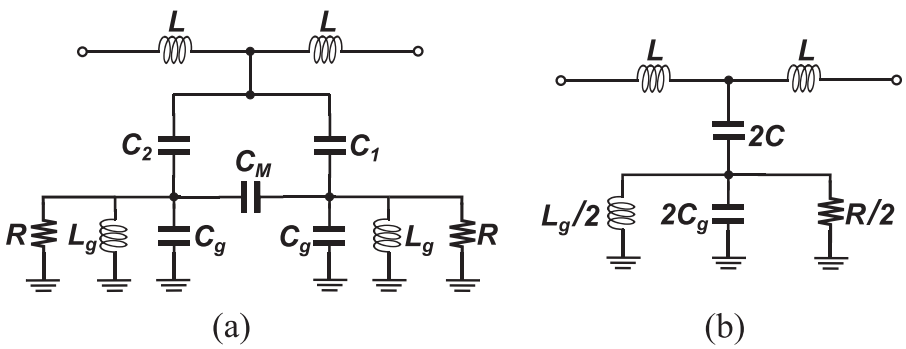

FIG. 5. (a) Lumped element circuit model of a microstrip line loaded with CELC2 resonator. (b) Simplified circuit model when the symmetry plane of the microstrip line is aligned with the electric wall of the resonator.

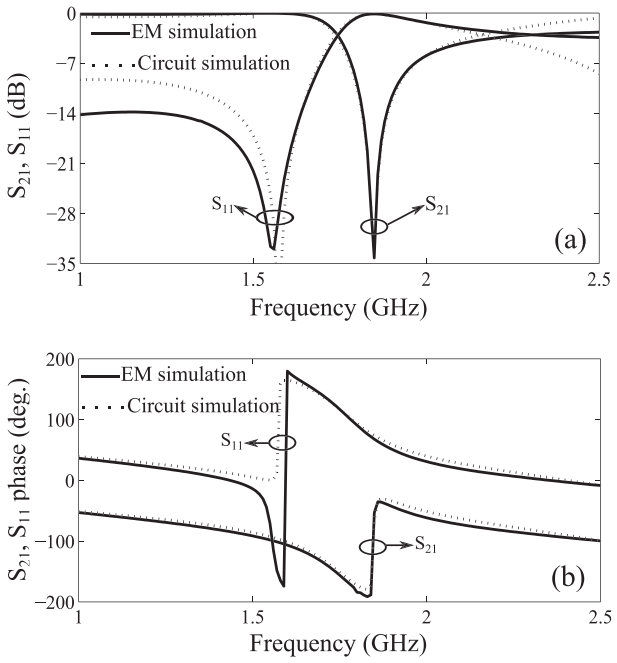

FIG. 6. Frequency response of the structure in Fig. 4(b) and its equivalent circuit model of Fig. 5(b). (a) Magnitude and (b) phase of the transmission and reflection coefficients. The resonator and microstrip line dimensions are listed in Fig. 4. The circuit parameters are: $L = 5.4$ nH, $C = 0.685$ pF, $C_g = 3.2$ pF, $L_g = 1.91$ nH, and $R = 7.5$ kΩ.

of C_M will be calculated by using Eq. (2) since the odd-mode resonance frequency is known from the electromagnetic simulations of the displaced structure. At this point, the reflection coefficient (S_{11}) will cross the unit impedance circle on the Smith chart again because (S_{11}) has two intersections with the unit impedance circle due to the dual-mode nature of the resonator. Afterwards, the values of C_1 and C_2 capacitances can be tuned by curve fitting of the electromagnetic and the equivalent circuit simulation results. The equivalent inductance of the transmission line L may be slightly modified in comparison to the aligned structure since the line inductance is affected by the resonator positioned beneath. The other element values are nearly unchanged. Here, we use the element values of the symmetric structure given in Fig. 6 as the initial values since the dimensions and the considered substrate are the same. The extracted circuit model parameters are listed in Table I for these three lateral displacements. The electromagnetic simulations results are shown together with the circuit model results in Fig. 7. As seen, there is a reasonable agreement between the EM and circuit simulations. The agreement validates the above analysis and the proposed circuit model in Fig. 5.

TABLE I. Extracted values of the equivalent circuit elements in Fig. 5(b) for three different displacements of the resonator.

Δx(mm)	L (nH)	C_1(pF)	C_2(pF)	C_M(pF)	C_g(pF)	L_g(nH)	R (kΩ)
0.6	4.15	1.05	0.34	1.73	3.2	1.9	7.5
1	4.15	1.14	0.25	1.85	3.2	1.9	7.5
2	4.15	1.18	0.09	2.05	3.2	1.9	7.5

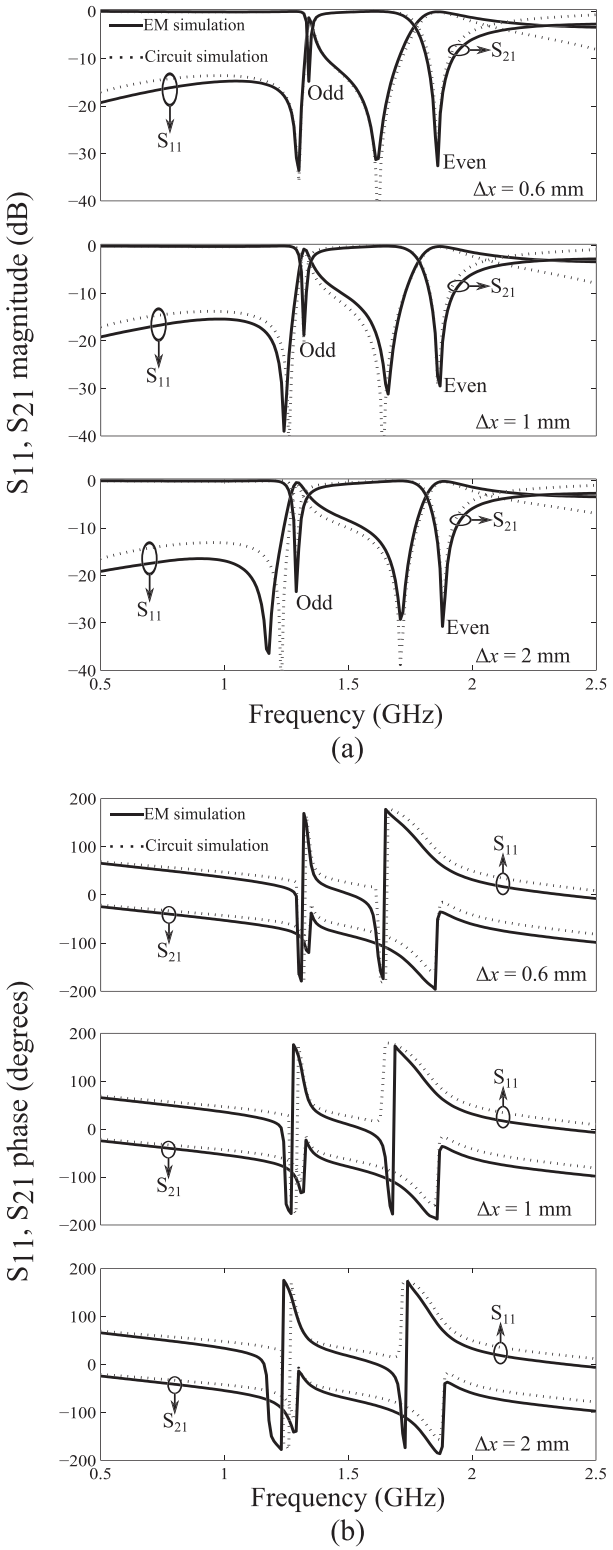

FIG. 7. Results from the electromagnetic and circuit simulations of the structure in Fig. 4(b) for three different displacements (0.6 mm, 1 mm, and 2 mm) of the resonator with respect to the microstrip line. (a) Magnitude and (b) phase of the transmission and reflection coefficients. The equivalent circuit parameters of the three cases are listed in Table I.

By looking at the plots in Figs. 6 and 7, it can be found that there are small discrepancies between the EM and circuit model simulations around the even-mode resonance, which takes place at higher frequencies. At these

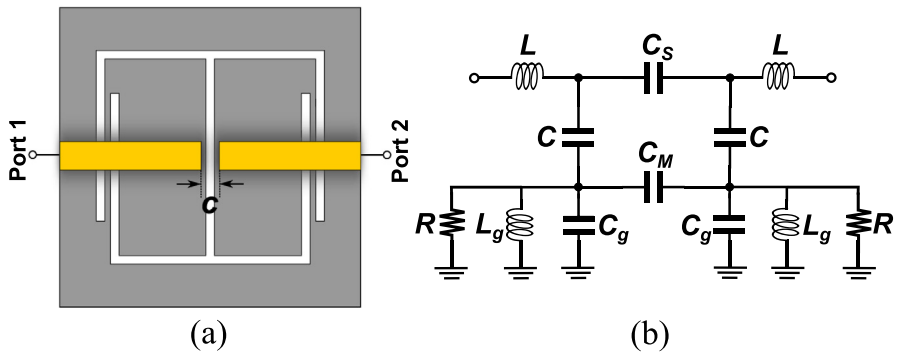

FIG. 8. Bandpass configuration of the CELC2 loaded microstrip line. (a) Layout of the structure. (b) Its equivalent circuit model.

frequencies, the wavelengths are shorter and closer to the resonator dimensions. As a result, the assumption of lumped elements becomes less accurate, and leads to the observable discrepancies.

B. Bandpass configuration

The bandstop response of the microstrip line loaded with the ELC2 resonator is associated with the negative permittivity of the structure around the resonance frequencies. This behavior can be easily changed to a bandpass response by introducing series capacitive gaps to the microstrip line.[24–26] The bandpass counterpart is demonstrated in Fig. 8 with its equivalent circuit model. The circuit model is very similar to the bandstop configuration excepting for C_S, which is added to the model to represent the capacitive gap of the microstrip line. Both of the C_1 and C_2 capacitors are considered to have the same value of C due to the symmetric alignment of the resonator and the transmission line. To extract the lumped element values in the circuit of Fig. 8(b), first, the bandstop version of Fig. 4 should be considered and simulated for obtaining L_g, C_g, and C_M values by using the procedure described in Sec. III A. The line inductance (L) can be estimated using a transmission line calculator or from the value obtained from the bandstop version in Fig. 4(b).

To obtain the values of C_S and C capacitors, the input impedance seen from the ports at the even-mode resonance frequency of the resonator should be considered. At the even-mode resonance frequency, the parallel branch of L_gC_g is open circuited and the equivalent circuit in Fig. 8(b) takes the form of Fig. 9 in which the input impedance seen from the ports can be calculated as

$$Z_{\text{in(even)}} = 50 + j2\omega_e L + \frac{1}{j\omega_e(C_S + C_{\text{eq}})}, \tag{4}$$

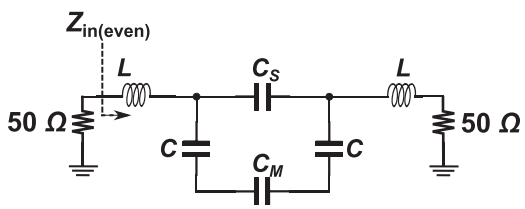

FIG. 9. Equivalent circuit of the bandpass configuration of microstrip line loaded with the CELC2 at the even-mode resonance frequency. The 50 Ω resistors indicate the input/output port impedance.

$$C_{\text{eq}} = \frac{CC_M}{C + 2C_M}, \tag{5}$$

where $\omega_e = 2\pi f_{\text{even}}$ that is known from the intersection of S_{11} with the normalized unit resistance circle in the Smith chart. On the other hand, by introducing the capacitive gap to the microstrip line, the odd-mode resonance frequency of the structure will be defined as

$$f_{\text{odd}} = \frac{1}{2\pi\sqrt{L_g(C_g + 2C_M + 2C_p)}}, \tag{6}$$

$$C_p = \frac{CC_S}{C + 2C_S}, \tag{7}$$

where f_{odd} is known from the intersection of the S_{11} with the unit resistance circle of the Smith chart. Thus, the values of C and C_S are calculated by using Eqs. (4) and (6). Note that because of the dual-mode nature of the resonator, the S_{11} has two intersections with the unit resistance circle of the Smith chart and the odd-mode intersection takes place in a lower frequency in comparison with the even-mode based on Eqs. (1) and (6). The bandpass structure in Fig. 8 has been simulated. A comparison between the electromagnetic and the equivalent circuit simulation results is presented in Fig. 10. The lumped element values of the equivalent circuit are extracted based on the procedure described above. The circuit simulations presented in Fig. 10 are in good agreement with the electromagnetic simulations. The results validate the proposed circuit model.

IV. POTENTIAL APPLICATIONS

The proposed configurations of CELC2 resonators loaded with microstrip lines can be used in designing new microwave devices in different ways. For example, the bandstop configuration in Fig. 4 can be used for implementing bandstop filters, where the rejection bandwidth can be improved by etching several resonators with slightly different sizes in the ground plane or by having identical resonators arranged with a small distance from each other to improve the inter-resonator coupling.[27] It has been shown that by displacing the resonator with respect to the microstrip line, the odd-mode resonance will also appear in the transmission response. This property can be used in designing dual bandstop filters,[28,29] where again the bandwidth can be widened by using multiple resonators that are accurately displaced with respect to the transmission line.

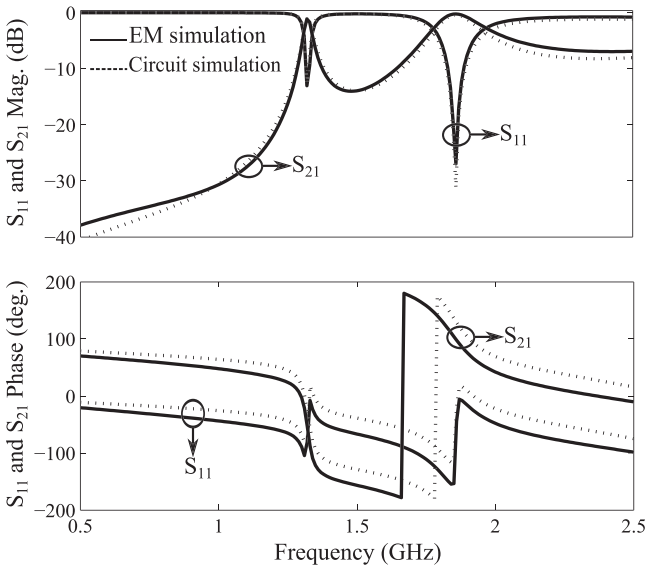

FIG. 10. Comparison between the electromagnetic and the equivalent circuit simulations of the bandpass configuration in Fig. 8. The resonator dimensions and the microstrip line width are the same as those given in Fig. 4. The considered capacitive gap width is $c = 0.2$ mm and the extracted equivalent circuit parameters are: $L = 4.4$ nH, $C_S = 28$ fF, $C_M = 1.91$ pF, $L_g = 1.91$ nH, $C_g = 3.13$ pF, and $R = 6$ kΩ.

It is known from Eq. (2) that the odd-mode resonance frequency is dependent on the value of the mutual capacitance between the two halves of the resonator (C_M). Thus, any change in the value of this capacitor can be detected from the frequency shift in the odd-mode notch in the transmission response (S_{21}) of the device. We can make use of this characteristic to design material characterization sensors by loading a dielectric sample onto this capacitive gap.[30–32]

Here, the performance of the presented structures is demonstrated by designing and characterizing a sensor and a filter. In the first case, the sensitivity to the CELC2 displacement is exploited for designing a displacement sensor, whereas in the second case, the bandpass configuration presented in Sec. III B is used for designing a dual-mode bandpass filter.

A. Displacement sensor design

It was demonstrated in Sec. III that displacing the CELC2 resonator with respect to the microstrip line excites the odd-mode resonance. The depth of the odd-mode transmission notch depends on the amount of displacement. This feature is used for designing a displacement sensor based on the presented bandstop configuration. Fig. 11(a) shows the top and bottom views of a prototype sample, where the CELC2 is displaced by 0.6 mm with respect to the microstrip line. Note that due to high sensitivity of the sensor to a small amount of displacement, the proposed sensor is verified through a number of fabricated samples with fixed displacement values.[33]

The measurement results of the sensor transmission coefficient (S_{21}) for the odd-mode transmission notch are shown in Fig. 11(b). As seen, the notch depth increases by increasing the resonator displacement. Although the odd-mode resonance frequency is slightly shifted due to displacement of the resonator, which in turn leads to complexity of the measurement setup, this frequency variation might be compensated by optimizing the resonator shape.[34] Additionally, optimizations may be carried out for improving other specifications of

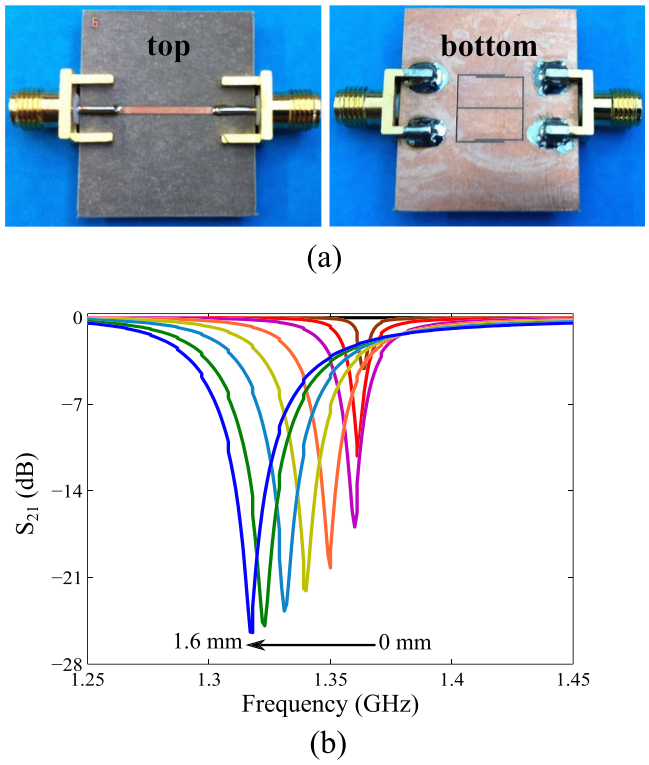

FIG. 11. Displacement sensor based on microstrip line loaded with the CELC2 resonator. (a) The fabricated sensor prototype. (b) Measurement results of the odd-mode resonance of the sensor for different displacements of the resonator with respect to the transmission line where, the displacement step is 0.2 mm. The resonator and transmission line dimensions are the same as the values given in Fig. 4.

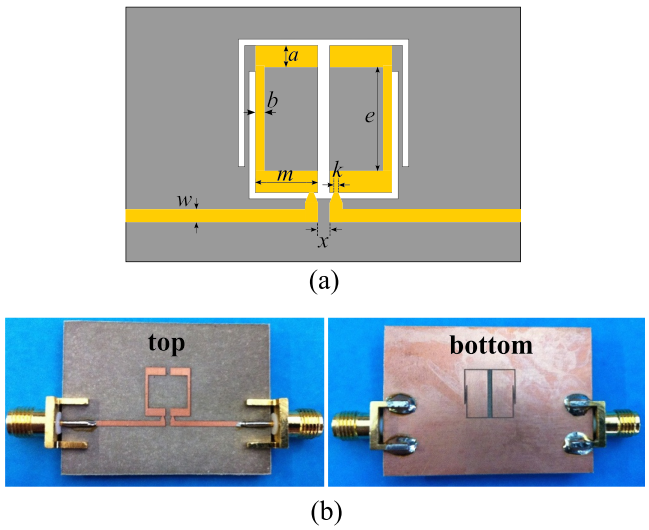

FIG. 12. The designed dual-mode bandpass filter based on the introduced bandpass configuration of microstrip line loaded with CELC2 resonator. (a) Layout of the filter with the yellow areas representing the top microstrip metalization and gray showing the bottom ground plane. (b) Photograph of the top and bottom view of the fabricated filter. The resonator parameters are all the same as the dimensions given in Fig. 4 except g, which is 1 mm here. The other dimensions are: $a = 1.5$ mm, $b = 0.5$ mm, $e = 6.6$ mm, $m = 4$ mm, $k = 0.2$ mm, $x = 1$ mm, and $w = 1$ mm.

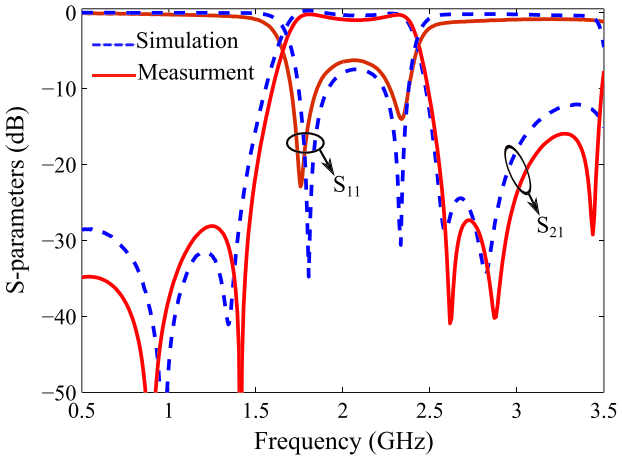

FIG. 13. Simulated and measured *S*-parameters of the designed dual-mode filter based on the presented bandpass configuration of CELC2 resonator loaded with microstrip line.

the sensor such as: sensitivity, dynamic range, linearity that are beyond the scope of this work.

B. Dual-mode bandpass filter design

Dual-mode filters are very attractive choices for RF and microwave systems due to their compact size.[25] Hence, the dual-mode bandpass configuration introduced in Sec. III B is utilized for implementation of a dual-mode bandpass filter here. The layout, along with the top and bottom views of the fabricated filter, is depicted in Fig. 12. The *C*-shaped input/output feeds are used for the filter to improve the passband response.[25,35]

The simulated and measured *S*-parameters of the designed filter from 0.5 GHz to 3.5 GHz are demonstrated in Fig. 13. The measurement shows a fractional bandwidth of 37% around the center frequency of 2 GHz. It should be mentioned that the fractional bandwidth is mainly determined from the difference between the even and odd-mode resonance frequencies of the resonator. From Eq. (4), this difference can be controlled by C_M or equivalently by changing g, which is the distance between the two halves of the resonator. The out-of-band rejection level of the filter is more than 30 dB. The overall size of the fabricated filter is $0.11\lambda_g \times 0.08\lambda_g$ implying a compact structure.

V. CONCLUSION

The dual-mode behavior of a special type of complementary electric-LC (CELC2) resonators loaded with microstrip line have been demonstrated and analyzed. Both of the bandpass and bandstop configurations have been introduced and their electromagnetic behaviors have been explained by using equivalent lumped-element circuit models. Their potential applications are discussed in the context of filters and sensors. A displacement sensor based on the bandstop structure and a dual-mode bandpass filter based on the bandpass configuration are designed and successfully validated.

[1]M. Durán-Sindreu, J. Naqui, J. Bonache, and F. Martín, Int. J. RF Microwave Comput.-Aided Eng. **22**, 439 (2012).
[2]F. Martín, J. Bonache, F. Falcone, M. Sorolla, and R. Marques, Appl. Phys. Lett. **83**, 4652 (2003).
[3]F. Falcone, T. Lopetegi, J. D. Baena, R. Marqués, F. Martín, and M. Sorolla, IEEE Microwave Wireless Compon. Lett. **14**, 280 (2004).
[4]M. Durán-Sindreu, J. Bonache, and F. Martín, IEEE Microwave Wireless Compon. Lett. **20**, 601 (2010).
[5]A. Vélez, F. Aznar, M. Durán-Sindreu, J. Bonache, and F. Martín, IET Microwaves, Antennas Propag. **5**, 277 (2011).
[6]A. Horestani, W. Withayachumnankul, A. Chahadih, A. Ghaddar, M. Zehar, D. Abbott, C. Fumeaux, and T. Akalin, IEEE Trans. Terahertz Sci. Technol. **3**, 851 (2013).
[7]A. Ebrahimi, W. Withayachumnankul, S. Al-Sarawi, and D. Abbott, IEEE Sens. J. **14**, 2609 (2014).
[8]J. Naqui, M. Durán-Sindreu, and F. Martín, Sensors **12**, 11790 (2012).
[9]A. K. Horestani, J. Naqui, Z. Shaterian, D. Abbott, C. Fumeaux, and F. Martín, Sens. Actuators, A **210**, 18 (2014).
[10]J. Naqui, A. Fernandez-Prieto, M. Duran-Sindreu, F. Mesa, J. Martel, F. Medina, and F. Martín, IEEE Trans. Microwave Theory Tech. **60**, 3023 (2012).
[11]G. Zamora, S. Zuffanelli, F. Paredes, F. Herraiz-Martinez, F. Martín, and J. Bonache, IEEE Antennas Wireless Propag. Lett. **12**, 1424 (2013).
[12]N. Takemura, IEEE Trans. Antennas Propag. **61**, 1891 (2013).
[13]J. Naqui, M. Durán-Sindreu, and F. Martín, Appl. Phys. A **115**(2), 637–643 (2014).
[14]J. Naqui, M. Durán-Sindreu, and F. Martín, Int. J. Antennas Propag. **2013**, 640514.
[15]J. Naqui and F. Martín, IEEE Trans. Microwave Theory Tech. **61**, 4700 (2013).
[16]W. Withayachumnankul, C. Fumeaux, and D. Abbott, IEEE Antennas Wireless Propag. Lett. **10**, 577 (2011).
[17]W. Withayachumnankul, C. Fumeaux, and D. Abbott, Opt. Express **18**, 25912 (2010).
[18]D. Schurig, J. Mock, and D. Smith, Appl. Phys. Lett. **88**, 041109 (2006).
[19]P. Yaghmaee, W. Withayachumnankul, A. Horestani, A. Ebrahimi, B. Bates, and C. Fumeaux, in *IEEE Antennas and Propagation Society International Symposium (APSURSI)* (2013), pp. 382–383.
[20]I. Gil, J. Bonache, M. Gil, J. García-García, F. Martín, and R. Marqués, J. Appl. Phys. **100**, 074908 (2006).
[21]J. Naqui, A. Fernández-Prieto, F. Mesa, F. Medina, and F. Martín, J. Appl. Phys. **115**, 194903 (2014).
[22]J. Bonache, M. Gil, I. Gil, J. García-García, and F. Martín, IEEE Microwave Wireless Compon. Lett. **16**, 543 (2006).
[23]F. Aznar, M. Gil, J. Bonache, L. Jelinek, J. Baena, R. Marqués, and F. Martín, J. Appl. Phys. **104**, 114501 (2008).
[24]M. Gil, J. Bonache, I. Gil, J. García-García, and F. Martín, Int. J. Numer. Modell.: Electron. Networks, Devices Fields **19**, 87 (2006).
[25]A. Ebrahimi, W. Withayachumnankul, S. Al-Sarawi, and D. Abbott, IEEE Microwave Wireless Compon. Lett. **24**, 152 (2014).
[26]A. Horestani, M. Durán-Sindreu, J. Naqui, C. Fumeaux, and F. Martín, IEEE Microwave Wireless Compon. Lett. **24**, 149 (2014).
[27]F. Martín, F. Falcone, J. Bonache, R. Marqués, and M. Sorolla, IEEE Microwave Wireless Compon. Lett. **13**, 511 (2003).
[28]A. M. Safwat, S. Tretyakov, and A. Räisänen, Microwave Opt. Technol. Lett. **49**, 1249 (2007).
[29]M. Zhou, C.-M. Tong, S.-H. Fu, L.-N. Wu, and X.-M. Li, in *2010 International Symposium on Signals Systems and Electronics (ISSSE)* (2010), Vol. 2.
[30]A. Ebrahimi, W. Withayachumnankul, S. Al-Sarawi, and D. Abbott, IEEE Sens. J. **14**, 1345 (2014).
[31]W. Withayachumnankul, K. Jaruwongrungsee, A. Tuantranont, C. Fumeaux, and D. Abbott, Sens. Actuators, A **189**, 233 (2013).
[32]M. Puentes, M. Maasch, M. Schussler, and R. Jakoby, IEEE Trans. Microwave Theory Tech. **60**, 1720 (2012).
[33]J. Naqui, M. Durán-Sindreu, and F. Martín, Sensors **11**, 7545 (2011).
[34]A. Horestani, D. Abbott, and C. Fumeaux, IEEE Sens. J. **13**, 3014 (2013).
[35]J.-C. Liu, D.-S. Shu, B.-H. Zeng, and D.-C. Chang, IET Microwaves, Antennas Propag. **2**, 622 (2008).